We are IntechOpen, the world's leading publisher of Open Access books Built by scientists, for scientists

4,800
Open access books available

122,000
International authors and editors

135M
Downloads

Our authors are among the

154
Countries delivered to

TOP 1%
most cited scientists

12.2%
Contributors from top 500 universities

CLARIVATE ANALYTICS BOOK CITATION INDEX INDEXED

WEB OF SCIENCE™

Selection of our books indexed in the Book Citation Index in Web of Science™ Core Collection (BKCI)

Interested in publishing with us?
Contact book.department@intechopen.com

Numbers displayed above are based on latest data collected.
For more information visit www.intechopen.com

Chapter 3

Oil Spill Pollution Automatic Detection from MultiSAR Satellite Data Using Genetic Algorithm

Maged Marghany

Additional information is available at the end of the chapter

http://dx.doi.org/10.5772/58572

1. Introduction

Oil spill pollution has a substantial role in damaging marine ecosystem. Oil spill that floats on top of water, as well as decreasing the fauna populations, affects the food chain in the ecosystem [1-5]. In fact, oil spill is reducing the sunlight penetrates the water, limiting the photosynthesis of marine plants and phytoplankton. Moreover, marine mammals for instance, disclosed to oil spills their insulating capacities are reducing, and so making them more vulnerable to temperature variations and much less buoyant in the seawater. Therefore, oil coats the fur of sea otters and seals, reducing its insulation abilities and leading to body temperature fluctuations and hypothermia. Ingestion of the oil causes dehydration and impaired digestions [5].

Over recent years, there has been explosive increments in marine oil spill pollutions. Deepwater Horizon oil spill in 2010, for instance, is the most serious marine pollution disaster has occurred in the history of the petroleum industry (Figure 1).

This disaster has dominated by three months of oil flows in coastal waters of the Gulf of Mexico. Incidentally, the Deepwater Hoizon oil spill has serious effects on feeble maritime, wildlife habitats, Gulf's fishing, coastal ecologies and tourism industries [30, 31]. Therefore, the resulting oil slicks are difficult to control, as their evolution be influenced by weather, currents, tides, and many chemical and physical factors [1][10][31]. Further, oil sources is challenging to verify and be subject to the type of oil, its volume and location, duration of the seepage, and surrounding environmental conditions [1].

Deepwater Horizon oil spill in 2010 is the most serious marine pollution disaster has occurred in the history of the petroleum industry. This disaster has dominated by three months of oil flows in coastal waters of the Gulf of Mexico. In this regard, the Deepwater Horizon oil spill has serious effects on feeble maritime, wildlife habitats, Gulf's fishing, coastal ecologies and

Figure 1. Oil spill disaster in Gulf of Mexico

tourism industries. As a result, human health problems are caused because of the spill and its clean-up [25]. Consistent with Marghany and Hashim [7], Synthetic aperture radar (SAR) is a precious foundation of oil spill detection, surveying and monitoring that improves oil spill detection by various approaches. The different SAR tools to detect and observe oil spills are vessels, airplanes, and satellites [5]. Vessels can detect oil spills at sea, covering restricted areas, say for example, (2500 m x 2500 m), when they are equipped with the navigation radars [20]. On the other hand, airplanes and satellites are the main tools that are used to record sea-based oil pollution [7] [22, 31].

1.1. Principle of oil spill detection in SAR data

The main theory of oil spill imaging using SAR images is based on the concept of resonance fundamental theory. Very short ocean waves travel on the larger ocean waves, or swells. As a superposition, radar backscatter at incident angles of 20° to 70° is principally produced by Bragg resonance [23].

1.1.1. General concept of Bragg scattering

According to According to Topouzelis [22] and Trivero [24], backscatter can model in two ways: specular reflection and Bragg scattering. Specular reflection occurs when the water surface is tilted which creates a small mirror pointing to the radar. For the perfect specular reflector, radar returns (backscatter) exist only near vertical incidence. This is because of a 90°-depression angle or the slope of the surface. In addition, the reflected energy is localized to the small angular region around the angle of reflection. Even for non-vertical incidence, however, backscatter can exist for a rough subsurface. This can occur if radar is penetrating deep enough[25]. Nevertheless, because of highest dielectric of water ocean, radar ‘s signal cannot penetrate sea surface.

http://dx.doi.org/10.5772/58572

Bragg or resonant scattering is scattering from a regular surface pattern. Resonant backscattering occurs when phase differences between rays backscattered from subsurface pattern interfere constructively. The resonance condition is $2\lambda_w \sin\theta=\lambda_r$, where λ_w and λ_r are water wavelength and the radar wavelength, respectively. θ is the local angle of incidence (Figure 2). According to Topouzelis et al., [20], the short Bragg-scale waves form in response to wind stress, if the sea surface is rippled by a light breeze and no long waves are present. The radar backscatter is due to the component of the wave spectrum. This resonates with a radar wavelength.

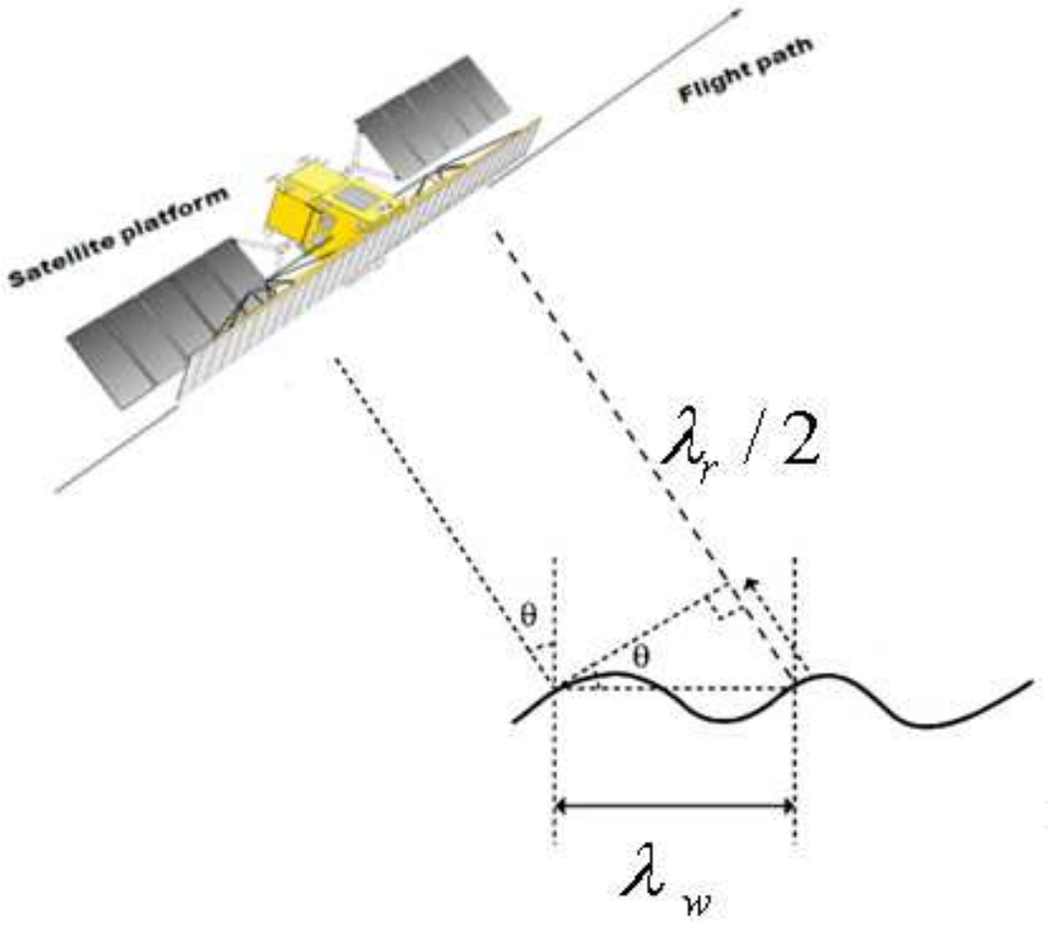

Figure 2. Bragg Scatter concept.

Swell waves being imaged have much longer wavelengths than the short gravity waves, which cause the Bragg resonance. Further, Bragg-resonance from the ocean might be considered as coming from facets. The term facet refers to a relatively flat portion of the long wave structure with cover of ripples containing Bragg-resonant facets. This behaves like specular points. The beam-width and scattering gain of each facet are determined by its length in the appropriate direction [4, 10, 22].

1.1.2. Mathematical expression of Bragg scattering

As the incidence angle of the SAR is oblique to the local mean angle of the ocean surface, there is almost no direct specular reflection except at very high sea states. It is therefore assumed that at first approximation Bragg resonance is the primary mechanism for backscattering radar pulses. The Bragg equation defines the ocean wavelengths λ_w for Bragg scattering as a function of radar wavelength λ_r and incidence angle θ :

$$\lambda_w = \frac{\lambda_r}{2\sin\theta} \tag{1}$$

The short Bragg-scale waves are formed in response to wind stress. If the sea surface is rippled by a light breeze with no long waves present, the radar backscatter is due to the component of the wave spectrum which resonates with the radar wavelength. The threshold wind speed value for the C-band waves is estimated to be at about 3.25 m/s at 10 meters above the surface. The Bragg resonant wave has its crest nominally at right angles to the range direction [3].

Under circumstance of Bragg scattering, largest incidence angle reduces the SAR backscatter. Indeed, the SAR backscattered power is proportional to the spectral energy density of the Bragg and the spectral distribution decays at shorter wavelength. SAR images tend to become darker with increasing range. Backscatter is related to the local incident angle (i.e. as the local incident angle increases, backscatter decreases), which is in turn related to the distance in the range direction. Backscatter is also related to wind speed [3].

According to Brekke and Solberg [3],For RADARSAT-1 and ENVISAT ASAR with C-band frequency, a radar wavelength of 5.7 cm and incidence angles in the range of 20^0-50^0 will this model give Bragg resonant sea wavelengths λ_w in the range of 8.3-3.7 cm. For surface waves with crests at an angle ϕ to the radar line-of-sight (Figure 3) the Bragg scattering criterion is

$$\lambda'_w = \frac{\lambda_r.\sin\phi}{2\sin\theta} = \lambda_w.\sin\phi \tag{2}$$

where λ'_w is the wavelength of the surface waves propagating at angle ϕ to the radar line-of sight. The resonant surface wavelengths will increase when frequency increases.

The SAR directly images the spatial distribution of the Bragg-scale waves. The spatial distribution may be effected by longer gravity waves, through tilt modulation, hydrodynamic modulation and velocity bunching. Moreover, variable wind speed, changes in stratification in the atmospheric boundary layer, and variable currents associated with upper ocean circulation features such as fronts, eddies, internal waves and bottom topography effect the Bragg waves [3, 22].

http://dx.doi.org/10.5772/58572

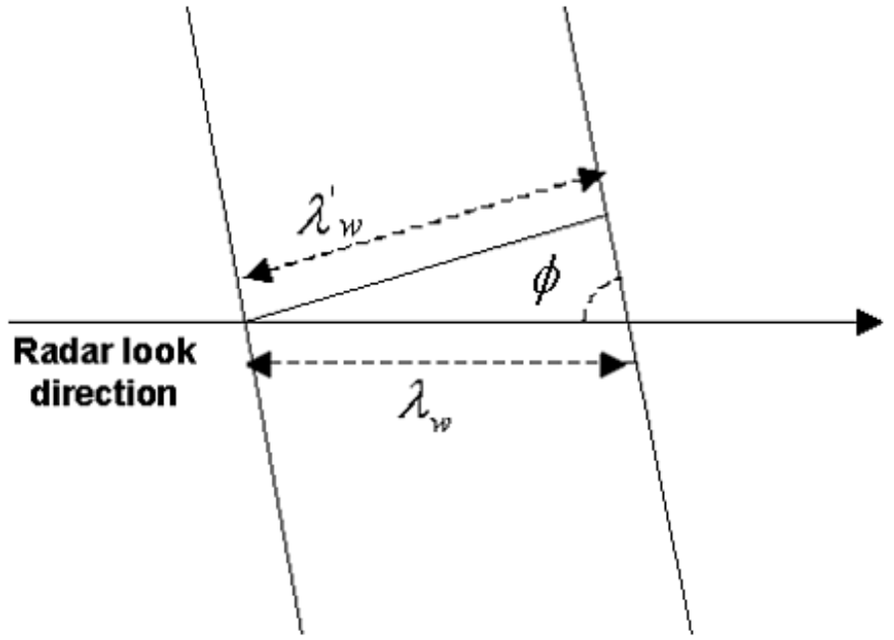

Figure 3. Crests at an angle ϕ to the look direction of the SAR [3].

1.1.3. Oil spill and surface films impact on Bragg scattering

Bragg scattering is a significant concept to understand the radar signal interaction with ocean surface. In this regard, the presence of capillary wave will produce backscatter that assists radar in imagining sea surface. Short gravity waves and capillary waves are damped by dynamic elasticity of the water surface, that is by changes in surface tension which occur when the surface is stretched or compressed [3]. This has the effect of the extracting of this energy from those waves which depends wholly or partly on surface tension to provide the restoring force necessary for wave propagation. If a surface film is present, the surface tension is lower than it would be in the absence of the film, and stretching and compression of the film because of the presence of waves provides the dynamic elasticity which enhances the wave damping. Thus capillary waves and short gravity waves are always damped in the presence of surface films [4]. If the surface film is spatially patchy,varying in thickness, or lined up in slicks because of surface convergence, it is to except that the capillary/gravity wave energy will reflect that patchiness, being greatest where is no surface film. Oil films on the sea surface damp the capillary waves of the surface height spectrum. This hydrodynamic damping influences the normalized radar cross section (NRCS) of contaminated seas, comparatively to clean seas [22].

Therefore, oil slicks dampen the Bragg waves (wavelength of a few cm) on the ocean surface and reduce the radar backscatter coefficient. This results in dark regions or spots in satellite SAR images. Topouzelis et al., [21], emphasizes the importance of weathering processes, as they influence the oil spills physicochemical properties and detect-ability in SAR images. The processes that play the most important role for oil spill detection are evaporation, emulsifica-

tion and dispersion. Lighter components of the oil will evaporate into the atmosphere. The rate of evaporation is dependent on oil type, thickness of the spill, wind speed and sea temperature. Emulsification is estimated based on water uptake as a function of the wind exposure of the actual oil type. Dispersion is an important factor in deciding the lifetime of an oil spill and it is strongly dependent on the sea state [3].

1.2. Oil spill detection in SAR data

Scientists which have agreed with that oil spill detection with SAR data is based on: (i) all dark patches present in the SAR images are isolated [3, 16]; (ii) features for each dark patch are then extracted [1, 12]; (iii) these dark patches are tested against predefined values [22]; and (v) the probability for every dark patch is calculated to determine whether it is an oil spill or a look-alike phenomenon [1, 14, 20, 22, 25]. Therefore, Topouzelis et al., [21] and Topouzelis [22] reported that most studies use the low resolution of SAR data such as quick-looks, with the nominal spatial resolution of 100 m x 100 m, to detect oil spills. In this regard, quick looks' data are sufficient for monitoring large scale area of 300 km x 300 km. On the contrary, they cannot efficiently detect small and fresh spills [22].

Further, SAR data have distinctive features as equated to optical satellite sensors which makes SAR extremely valuable for spill watching and detection [5] [7] [9] [13]. These features are involved with several parameters: operating frequency, band resolution, incidence angle and polarization [10] [12]. Marghany and Hashim [7] develop comparative automatic detection procedures for oil spill pixels in Multimode (Standard beam S2, Wide beam W1 and fine beam F1) RADARSAT-1 SAR satellite data post the supervised classification (Mahalanobis), and neural network (NN) for oil spill detection. They found that NN shows a higher performance in automatic detection of oil spill in RADARSAT-1 SAR data as compared to the Mahalanobis classification with a standard deviation of 0.12. In addition, they W1 beam mode is appropriate for oil spill and look-alikes discrimination and detection [10] [11] [12]. Recently, Skrunes et al., [9], nevertheless, reported that there are several disadvantages are associated with Current SAR based oil spill detection and monitoring. They stated that, SAR sensors are not able to detect thickness distribution, volume, the oil-water emulsion ratio and chemical properties of the SAR data. In this regard, they recommended to utilize multi-polarization acquisition data such as RADARSAT-2 and TerraSAR-X satellites. They concluded that the multi-polarization data show a prospective for prejudice between mineral oil slicks and biogenic slicks.

Finally Marghany, [30] used Genetic algorithm for oil spill detection in ENVISAT ASAR data along Singapore Straits. He found that crossover process, and the fitness function generated accurate pattern of oil slick in SAR data. He used the receiver –operational characteristics (ROC) curve to verify oil spill detection in SAR data. He stated that ROC verified 85% for oil spill, 5% look–alikes and 10% for sea roughness.

1.3. Problem statement

The main challenge with SAR satellite data is the difficulty to drawbacks, which makes it difficult to develop a fully automated detection of oil spills. Due to the inherent difficulty of

http://dx.doi.org/10.5772/58572

discriminating between oil spills and look-likes, an automatic algorithm with a reliable confidence estimator of oil spill would be highly desirable. The needs for automatic algorithms rely on the number of images to be analyzed, but for monitoring large ocean areas, it is a cost-effective alternative to manual inspection. Automatic detection algorithms of oil spill are normally divided into three steps: (i) dark spot detection; (ii) dark spot feature extraction; and (iii) dark spot classification [3,10, 22,31].

One of the main problems in oil slick combat and management are forecasting the behavior (movement and spreading) of oil slicks. Commonly, the objective of predicting the behavior of oil slicks is to determine the time-evolving shape of the slick under different weather patterns in waters where currents exist [11-14]. Wind direction and speed are the most important climate parameters can impact the oil spill imagine in SAR data. Although great progress made in detecting and surveying oil slicks, a general model for oil slick movement and spreading has not yet been devised [1]. Models for oil slick behavior are important in environmental engineering and used as a decision support tool in environmental emergency responses. These models also use to help ships avoid oil slicks [1].

Modeling the progress and extent of oil in the ocean are not always tested against authentic spills, and models are not regularly developed with real databases, but rely instead on theoretical scenarios. In fact, some spill-threat scenarios have not been based on real oil movement data at all [15]. Yet there are frequent demands to provide just such models with credible precision. Consequently, it is important to study the behavior and movement of spilled oil in the sea in order to describe a suitable management plan for mitigating adverse impacts arising from such accidents. Simulation of oil spills using mathematical models form an important basis for subsequent study, according to Marghany [9]. Collectively, with the information of position of weak resources in time and space, the simulation outcome may develop a basis for evaluating the damage potential from an eventual oil spills. This may help the regulatory authorities to take direct preventive measures [9].

In addition, most of the studies that have been conducted in the coastal waters of Malaysia used a single radar image, which is inadequate to ensure a high degree of accurate detection of oil spills using SAR data. Some of the work involved the implementation of non-appropriate techniques for oil spill automatic detection. For instance, Mohamed et al., [16] have used data fusion techniques in a single RADARSAT-1 SAR image, with different co-occurrence texture algorithm results. However, the data fusion technique must apply with two or more different sensors for example, ERS-1, LANDSAT, and SPOT. In addition, according to Brekke and Solberg [3], using such PCA analysis does not consider an appropriate method for data fusion. Data fusion technique involves several methods such as high pass filtering technique, IHS transformation method, Brovey method, and à Trous wavelet method [3].

1.4. Hypotheses and objective

Concern with above prospective, we address the question of Genetic algorithm ability for oil spill detection in multiSAR satellite. This work has hypothesized that the dark spot areas (oil slick or look-alike pixels) and its surrounding backscattered environmental signal complex looks in the ENVISAT ASAR data can detect using Genetic Algorithm. However, previous

work has implemented post classification techniques [4, 9, 16, 18] or artificial neural network [19],[21],[24] which are considered as semi-automatic techniques. The objective of this work can divide into two sub-objectives: (i) To examine GA [27, 31] for oil spill automatic detection in multiSAR satellite data; and (ii) To design the multi-objective optimization algorithm for oil spill automatic detection in multiSAR satellite data that are based on algorithm's accuracy.

2. Data acquisition

The SAR data acquired in this study are from the ENVISAT ASARR and RADARSAT-2 SAR data that are involved Standard beam mode (S2); W1 beam mode (F1) image. SAR data are C-band and have a lower signal-to noise ratio due to their HH polarization with wavelength of 5.6 cm and a frequency of 5.3 GHz [7]. Further, RADARSAT-SAR data have 3.1 looks and cover an incidence angle of 23.7° and 31.0° [10]. In addition, RADARSAT-2 SAR data cover a swath width of 100 km.

SAR operation modes	
Frequency range	C-band (5.405 GHz)
Channel bandwidth	11.6, 17.3, 30, 50 and 100 MHz
Channel polarization	HH, HV, VH, VV
SAR antenna dimensions	15m x 1.5m

Table 1. RADARSAT-2 SAR different mode.

ASAR (Advanced Synthetic Aperture Radar) operates in the C band in a wide variety of modes. It can detect changes in surface heights with sub-millimeter precision. It served as a data link for ERS-1 and ERS-2, providing numerous functions such as observations of different polarities of light or combining different polarities, angles of incidence and spatial resolutions (Table 2).

Mode	Id	Polarisation	Incidence	Resolution	Swath
Alternating polarisation	AP	HH/VV, HH/HV, VV/VH	15 – 45°	30 – 150 m	58 – 110 km
Image	IM	HH, VV	15 – 45°	30 – 150 m	58 – 110 km
Wave	WV	HH, VV		400 m	5 × 5 km
Suivi global (ScanSAR)	GM	HH, VV		1 km	405 km
Wide Swath (ScanSAR)	WS	HH, VV		150 m	405 km

Table 2. ENVISAT different Modes.

http://dx.doi.org/10.5772/58572

3. Study area

The study conducted in two different coastal zones. The first area is located along the Gulf of Mexico and the second is located along Singapore Straits. It is surprising that the two oil spill disaster events occurred in April 20, 2010, and May 25, 2010, respectively.

3.1. Gulf of Mexico

The Deepwater Horizon, an offshore oil-drilling rig, exploded on the night of April 20, 2010 while working on a well on the sea floor in the Gulf of Mexico. The blast occurred 41 miles from the Louisiana coast (Figure 5). For nearly three months, oil leaked from the Macondo well at a rate estimated between 35,000 and 60,000 barrels per day. (There are 42 gallons in a barrel, so that's equal to 1.4 to 2.5 million gallons per day.) Repeated attempts to stop the flow failed until mid-July, when a tighter-fitting cap sealed the well head. In all, the well spilled 4.9 million gallons: the biggest offshore oil spill in history. Further, the oil slick spread quickly over the ocean surface, covering 1,500 square kilometers (580 sq miles) by April 25 and over 6,500 square kilometers (2,500 sq miles) by the beginning of May.

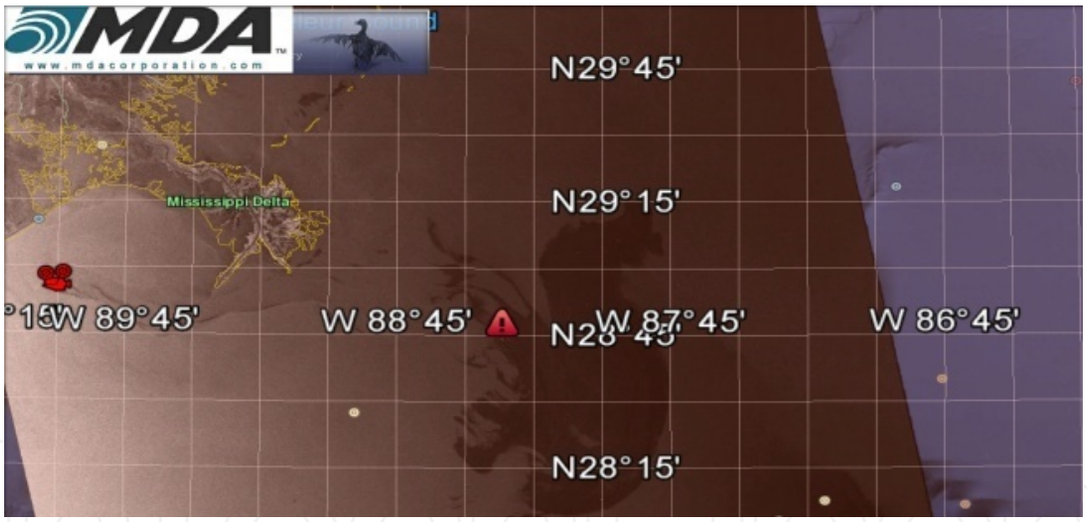

Figure 4. Location of oil spill event in Gulf of Mexico.

3.2. Singapore straits

The second study area is located along the Singapore Straits. The SAR data acquired in this study are from ENVISAT ASAR data on June 3, 2010, in single look complex format. On May 25, 2010 a merchant ship (Figure 6) collided with a Malaysian oil tanker on Tuesday morning, puncturing the tanker's hull and spilling 2,500 tons of crude oil into the Singapore Strait (Figure 7), maritime officials reported. The damage appeared to be limited to one compartment in the double-hulled tanker, the Bunga Kelana 3, with the spill amounting to about 18,000 barrels.

Figure 5. The merchant ship collided with a Malaysian oil tanker.

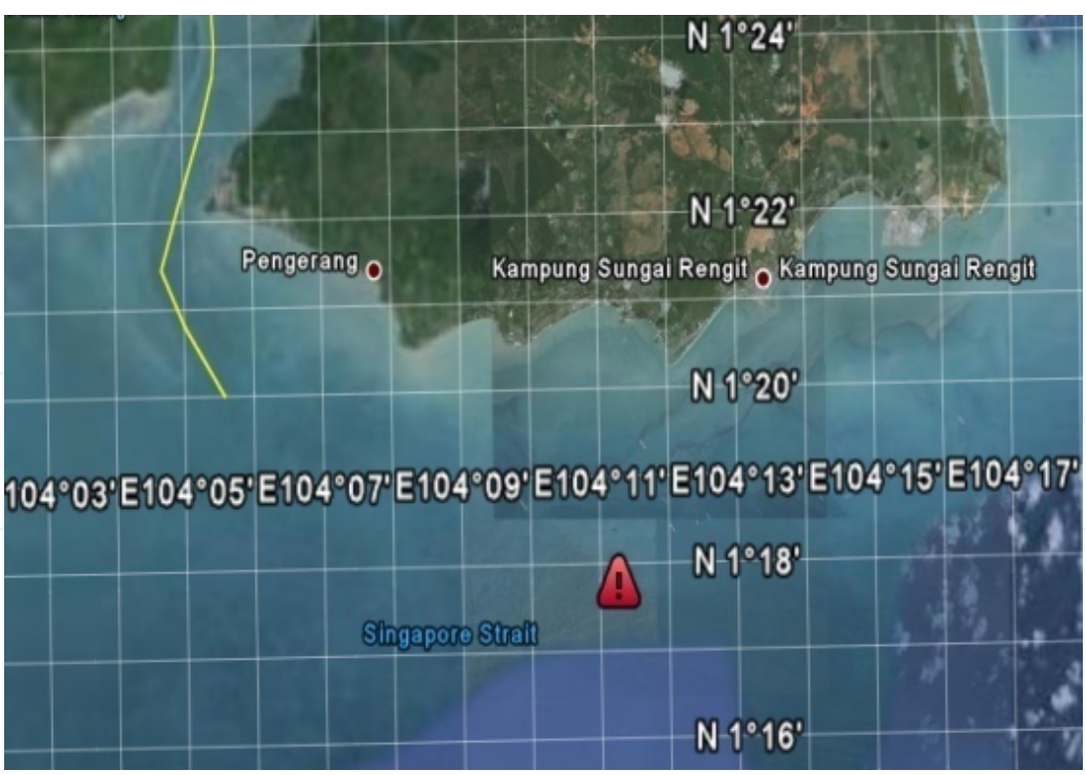

Figure 6. Location of oil spill is shown by red triangular.

http://dx.doi.org/10.5772/58572

4. Genetic algorithm

On the word of Kahlouche et al., [27], Genetic algorithms (GA) differ from classification algorithm. In classification algorithm, a single point at every iteration is generated. Moreover, classification algorithms correspondingly choose the next point in the classification by a deterministic computation. In contrast, the genetic algorithm (GA) generates a population of cells at every iteration, where the superlative cell in the population approaches an optimal solution. Moreover, GA, implements probabilistic transition rules not deterministic rules as compared to classification algorithms [22] [28, 31]. Consequently, Cellular Automata (CA) are mathematical algorithms that involve a large number of relatively simple individual units, or "cells," which is connected only locally, without the existence of a central control in the system. Each cell is a simple finite automaton that repeatedly updates its own state, where the new cell state depends on the cell's current state and those of its immediate (local) neighbors. The limited functionality of each cell, and the interactions, however, being restricted to local neighbors. Thus the system as a whole is capable of producing intricate patterns, and performing complicated computations [29].

A constrained multi-objective problem for oil spill discrimination in SAR data deals with more than one objective and constraint namely look-alikes, for instance, currents, eddies, upwelling or downwelling zones, fronts and rain cells). The general form of the problem is adapted from Sivanandam and Deepa [29] and described as

Minimize

$$f(\beta) = [f_1(\beta), f_2(\beta), ..., f_k(\beta)]^T \tag{3}$$

Subject to the constraints:

$$g_i(\beta) \le 0, i = 1,2,3,..I \tag{4}$$

$$h_j(\beta) \le 0, j = 1,2,3,...J \tag{5}$$

$$\beta_s \le \beta \le \beta_U \tag{6}$$

where, $f_i(\beta)$ is the *i-th* pixel backscatters β in SAR data, $g_i(\beta)$ and $h_j(\beta)$ represents the *i-th* and *j-th* constraints of backscatter in raw direction and column direction, respectively. β_L and β_U are the lower and upper limit of values of the backscatter.The transition rules for the cellular automata oil spill detection is designed using the input of different backscatter values β to identify the slick conditions required in the neighbourhood pixels of kernel window size of 7x7 pixels and lines for a β pixel to become oil slick. These rules can be summarized as follows:

1. IF test pixel is sea surface, OR current boundary features THEN $\beta \geq 0$ not oil spill.
2. IF test pixel is dark patches (low wind zone, OR biogenic slicks OR shear zones) $\beta \leq 0$THEN It becomes oil slick if its.

4.1. Data organization

Let the entire backscatter of dark patches in multiSAR data are β_1, β_2, β_3, ..., β_k where K is the total number backscatter of dark patches in the multiSAR data. Therefore, K is made up from genes which is representing the backscatter β of dark patches and its surrounding environment and genetic algorithms is started with the population initializing step.

4.2. Population initializing

Let P_i^j is a gene which corresponds to backscatter of dark pixels and its surrounding pixels. Consequently, P_i^j is randomly selected and representing both of backscatter variations of dark patches and its surrounding environmental pixels. Moreover, i varies from 1 to K and j varies from 1 to N where N is the population size.

4.3. The fitness function

Following Kahlouche et al., [27], a fitness function is selected to determine the similarity of each individual backscatter of dark patches in RADARSAT-2 SAR and ENVISAT ASAR data. Then the backscatter of dark patches in RADARSAT-2 SAR and ENVISAT data be symbolized by β_i where i=1,2,3, …, K and the initial population P_i^j where j=1,2,3, …, N and i=1,2,3…, K. Formally, the fitness value $f(P^i)$ of each individual of the population is computed as follows [27]:

$$f(P^j) = [\sum_{i=1}^{K} \left| P_i^j - \beta_i \right|]^{-1} \quad j = 1, \ \ldots, N. \tag{7}$$

where, N and K are the number of individuals of the population used in fitness process. Generally, Equation 7 used to determine the level of similarities of dark patches that are belong to oil spill in RADARSAT-2 SAR and ENVISAT ASAR data.

4.4. Selection step

The key parameter in the selection step of genetic algorithm which is chosen the fittest individuals $f(P^j)$ from the population P_i^j. The threshold value τ is determined by the maximum values of fitness of the population $Max\ f(P^j)$ and the minimum values of fitness of the population of $Min\ f(P^j)$ Indeed, in the next generations, this step serves the populations P. Therefore, the values of the fittest individuals dark patches in RADARSAT-2 SAR and ENVISAT ASAR data are greater identifies threshold τ which is given by

http://dx.doi.org/10.5772/58572

$$\tau = 0.5\ [Max\ f(P^j) + Min\ f(P^j)] \tag{8}$$

Equation 8 used as selection step to determine the maximum and minimum values of fitness of the population, respectively. This is considered as a dark patches' population generation step in GA algorithm.

4.5. The reproduction step

According to Sivanandam and Deepa [29], Genetic algorithm is mainly a function of the reproducing step which involves the crossover and mutation processes on the backscatter population P_i^j in SAR data. In this regard, the crossover operator constructs the P_i^j to converge around solutions with high fitness. Thus, the closer the crossover probability is to 1 and the faster is the convergence [27]. In crossover step the chromosomes interchange genes. A local fitness value effects each gene as

$$f(P_i^j) = \left| \beta_i - P_i^j \right| \tag{9}$$

Then the crossfire between two individuals consists to keep all individual populations of the first parent which have a local fitness greater than the average local fitness $f(P_{av}^j)$ and substitutes the remained genes by the corresponding ones from the second parent. Hence, the average local fitness is defined by:

$$f(P_{av}^j) = \frac{1}{K} \sum_{i=1}^{K} f(P_i^j) \tag{10}$$

Therefore, the mutation operator denotes the phenomena of extraordinary chance in the evolution process. Truly, some useful genetic information regarding the selected population could be lost during reproducing step. As a result, mutation operator introduces a new genetic information to the gene pool [27].

4.5.1. Morphological operations

Morphological operation on the selected individuals is performed prior to the cross-over and the mutation process. This is to exploit connectivity property of the RADARSAT-2 SAR and ENVISAT ASAR data [28]. The morphological operators are implemented through reproduction step: (i) closing followed by (ii) opening. In this regard, the accuracy of dark patch segmentations are function of the size and the shape of the structuring element. Therefore, kerneal window size of a square of structuring of 7 x 7 is chosen to preserve the fine details of oil spill in RADARSAT-2 SAR and ENVISAT ASAR data [29, 31].

5. Results and discussion

5.1. Gulf of Mexico

In this study, RADARSAT-2 SAR data with RADARSAT-2 in ScanSAR Narrow B Beam on April 28, 2010 at 11:51:29 UTC is implemented for oil spill detection in the Gulf of Mexico. The Satellite has a Synthetic Aperture Radar (SAR) with multiple polarization modes, including a fully polarimetric mode in which HH, HV, VV and VH polarized data are acquired. Its highest resolution is 1 m in Spotlight mode (3 m in Ultra Fine mode) with 100 m positional accuracy requirement. In ScanSAR Wide Beam mode the SAR has a nominal swath width of 500 km and an imaging resolution of 100 m. An oil platform located 70 km from the coast of Louisiana sank on Thursday April 22, 2010 in the Gulf of Mexico spilling oil into the sea [9].

On these RADARSAT image we can clearly see the evolution of the spill, which has a darker tone than the surrounding water, as well as some boats in the area (Figure 8a). Figure 8 b shows the ENVISAT ASAR data was acquired on May 9, 2010. These data are C-band and had the lower signal-to-noise ratio owing to their HH polarization with a wavelength range of 3.7 to 7.5 cm and the frequency of 5.331 GHz. ASAR can achieve a spatial resolution generally around 30 m. The ASAR is intended for applications which require the spatial resolution of spatial resolution of 150 m. This means that it is not effective at imaging areas in depth, unlike strip map SAR. The azimuth resolution is 4 m, and range resolution is 8 m. This confirms the study of Marghany [31] and [32].

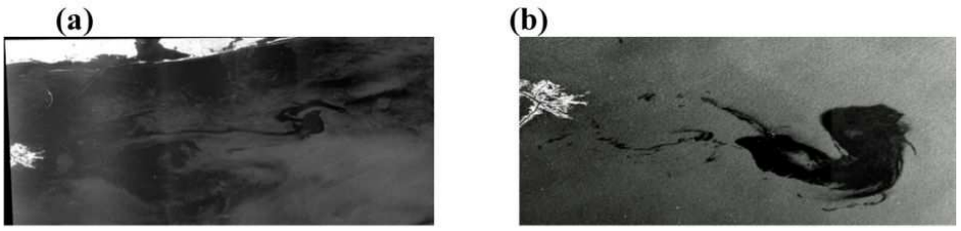

Figure 7. MultiSAR data over Gulf of Mexico (a) RADARSAT-2 SAR and (b) ENVISAT ASAR data

5.2. Singapore straits

Figure 9 shows the ENVISAT ASAR was acquired on June 3rd 2010 after the Merchant ship collided with a Malaysian oil tanker near the Singapore and Malaysian coastal waters. Clearly, there are various of dark patches which are scattered over a large area of coastal waters. The lowest backscatter of-40 dB,-45dB,-50dB are noticed in areas A, B and C, respectively. The highest backscatter of-10 dB is represented ships in area D (Figure 10). In fact, oil spills change the roughness of the ocean surface to smoothness surface which appear as dark pixels as compared to the surrounding ocean [1-22]. Therefore, the speckle caused difficulties in dark patch identifications in SAR data [14, 16]. Further, wind speed was recorded during 3rd June 2010 was ranged between 1 to 6 m/s.

http://dx.doi.org/10.5772/58572

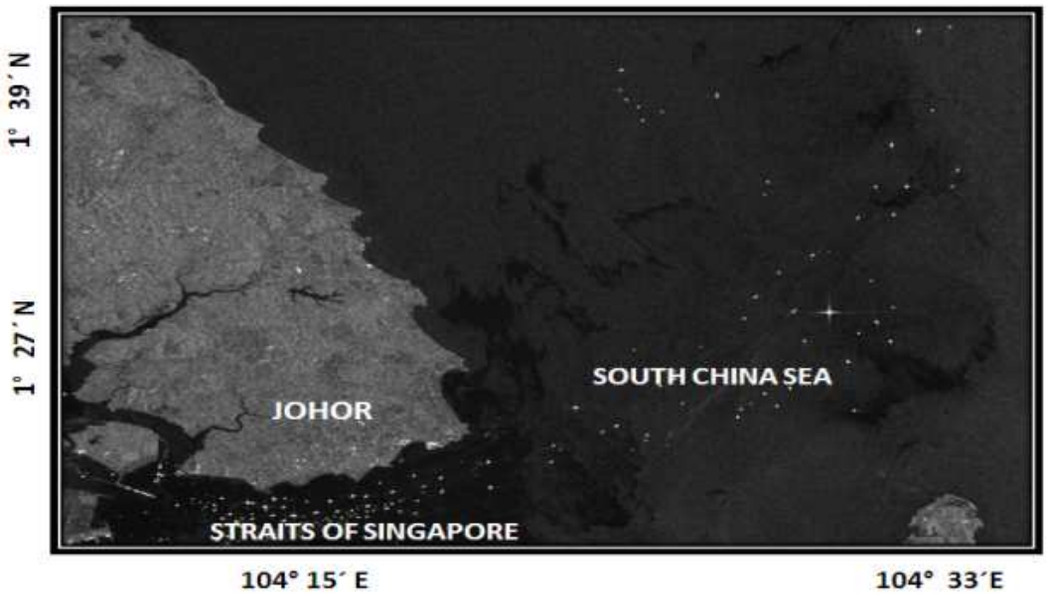

Figure 8. ENVISAT ASAR data during 3rd June 2010 along Straits of Singapore and South China Sea.

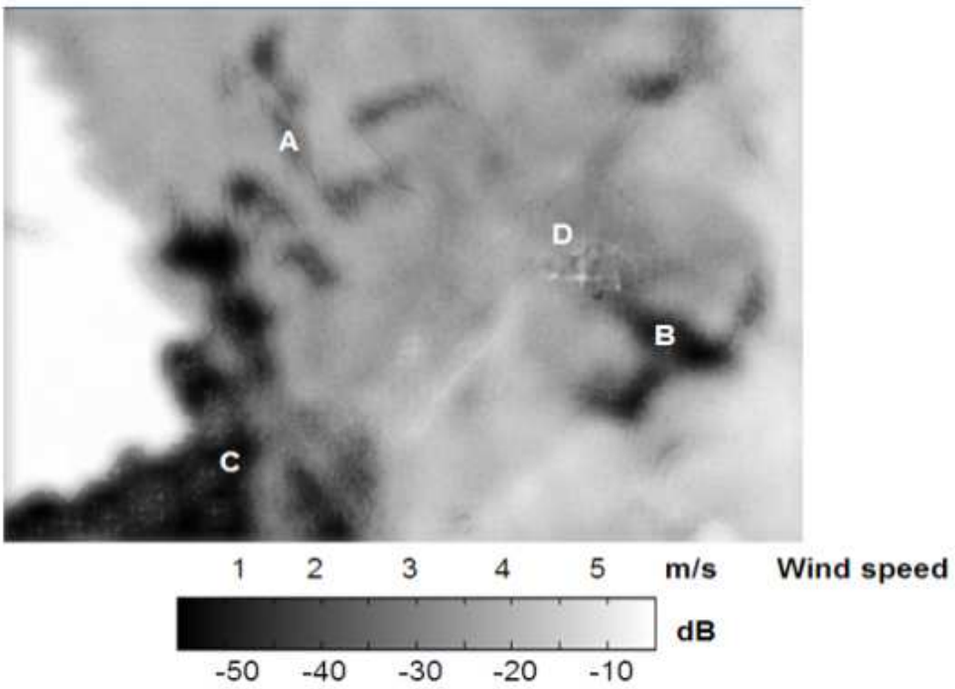

Figure 9. Backscatter and wind speed variations in ENVISAT ASAR data.

5.3. Genetic algorithm output

However, the result of backscatter values is different as compared to previous studies of Marghany et al., [10] [11] and Marghany and Hashim [12]. This is because of previous studies used different radar sensor of the RADARSAT-1 SAR and these studies have done under different weather and ocean conditions compared to recent work. Figure 11 shows example of the crossover process with 10 individuals. In this 10 individuals, the positive dark patches are represented oil spill pixels while negative dark patches represent the surrounding pixels. Accordingly, every cellular is compared with the corresponding cell in the others to determine either to be positive or negative.

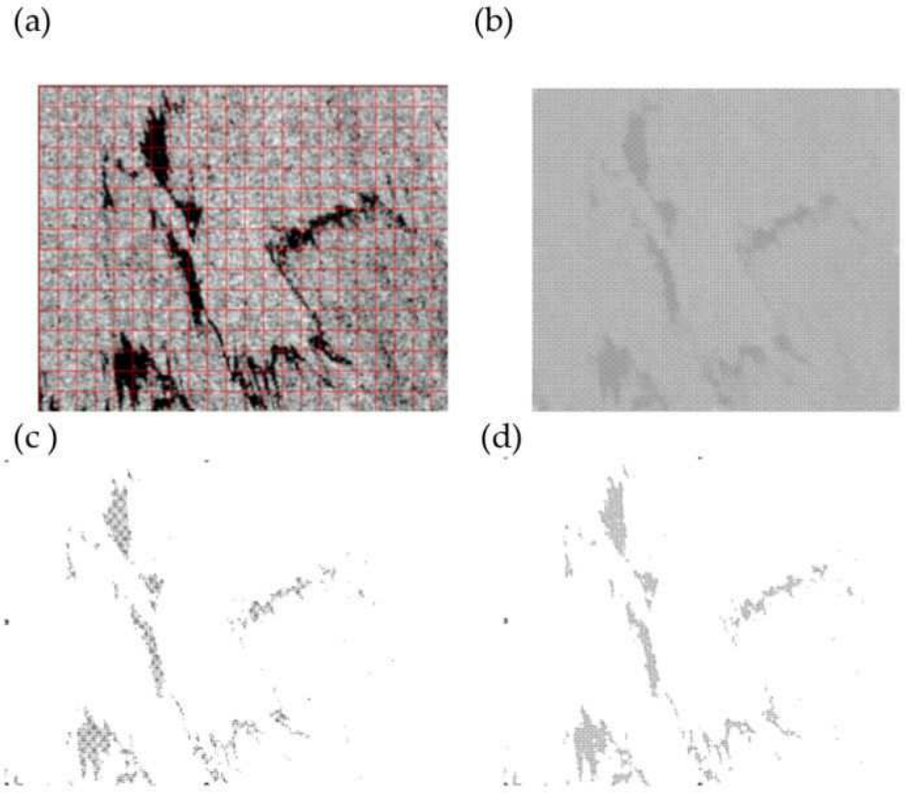

Figure 10. Crossover procedures (a) original data, (b) first individual, (c) resulting from an individual prior cancellation, and (d) after cancellation.

In these procedures, cell has a positive value and must be strengthened when cell in the intermediate prototype has a value larger than zero and greater than threshold 's value. In this regard, these cells are represented an oil spill event in ENVISAT ASAR data. On the contrary, the cell represents look-alikes when it has a negative value. As a result, the cell in the intermediate prototype is less than zero and threshold 's value. In this regard, this cell must be diminished. The variation cell value (positive or negative) is a function of dissimilarity of the comparable cells. This study confirms and extends the capabilities of GA introduced by Kahlouche et al., [27].

http://dx.doi.org/10.5772/58572

Clearly the genetic algorithm is able to isolate oil spill dark pixels from the surrounding environment. In other words, look-alike, low wind zone, sea surface roughness, and land are marked by white colour while oil spill pixels are marked all black(Figures 12 and 13). Further, Figures 12 and 13 show the results of the GA, where 100% of the oil spills in the test set were correctly classified. This study is not similar to previous work done by Marghany and Hashim [12]. The dissimilarity is because this work provides the automatic classifier based on GA but Marghany and Hashim work is considered as a semi-automatic tool for oil spill detection.

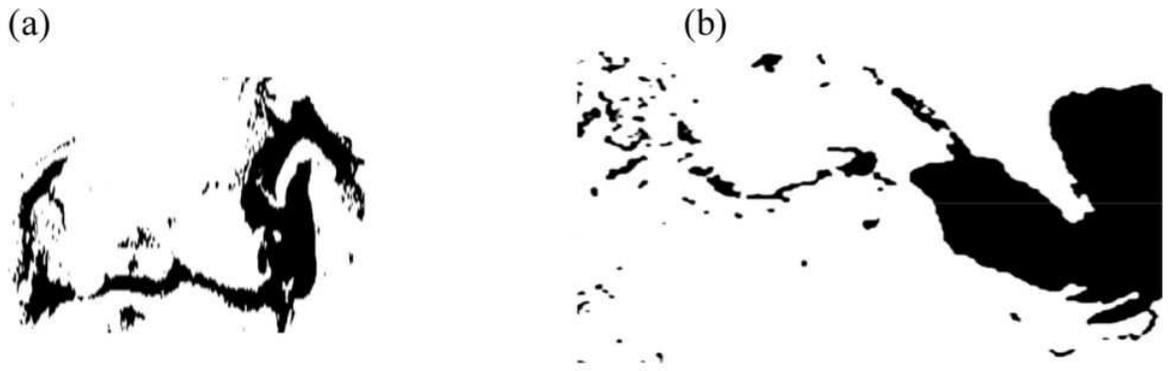

Figure 11. Oil spill automatic detection by Genetic Algorithm (GA) using (a) RADARSAT-2 SAR and (b) ENVISAT ASAR in Gulf of Mexico

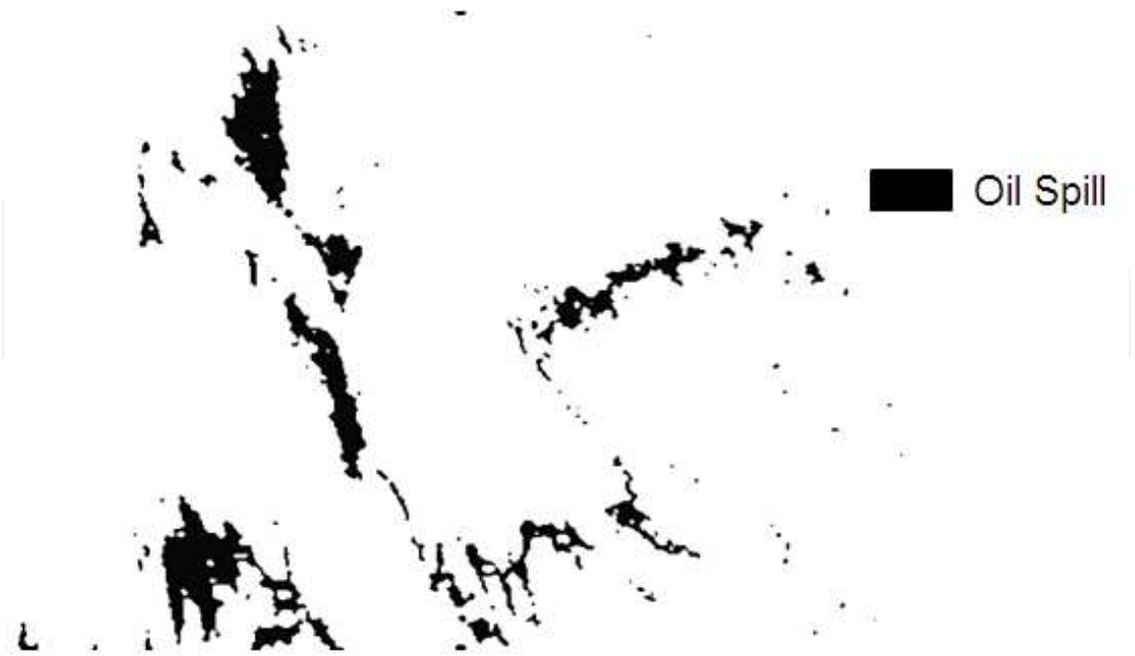

Figure 12. Oil spill automatic detection by Genetic Algorithm (GA) in Singapore Straits

The receiver–operator characteristics (ROC) curve in Figure 14 indicates a significant difference in the discriminated between oil spill, look-alikes and sea surface roughness pixels. In terms of ROC area, the oil spill has an area difference of 85% and 5% for look – alike and 10% for sea roughness and a ϱ value less than 0.0005 which confirms the study of Marghany et al., [10] [11]. This suggests that genetic algorithm is an excellent classifier to discriminate region of oil slicks from surrounding water features. This conforms the study of Marghany [30] and [31].

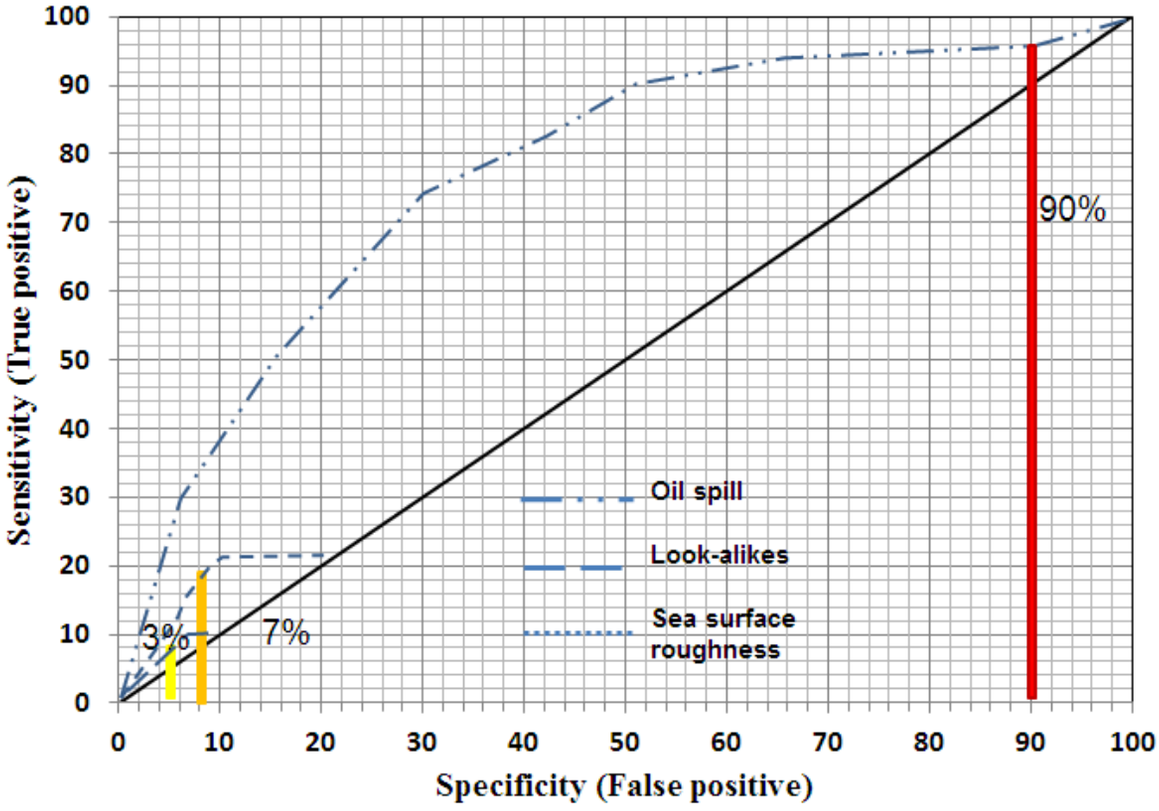

Figure 13. ROC for oil spill discrimination using Genetic Algorithm (GA).

In general, genetic algorithm contains the crossover procedure. In this regard, a new population is generated in each crossover process. As a result, individual populations are examined by the fitness function and added to the population. Thus, new populations are continuously generated based on the dissimilarities between the two successive fitness values. In addition, the crossover procedure produced a more refined oil spill pattern by despeckle and maintenance the morphology of oil spill pattern features. This is because of the fitness function is used to sustenance the oil spill pixel classification. Indeed, fitness function selected oil spills morphological pattern which is close to the requested spill prototype.

http://dx.doi.org/10.5772/58572

In contrast to previous studies of Fiscella et al., [4] and Marghany and Mazlan [13], the Mahalanobis classifier provides a classification pattern of oil spill where the slight oil spill can distinguish from medium and heavy oil spill pixels. Nevertheless, this study is consistent with Topouzelis et al., [20-22]. In consequence, the genetic algorithm extracted oil spill pixels automatically from surrounding pixels without using different segmentation algorithm as stated at Solberg et al., [19]; Samad and Mansor [18];Marghany and Mazlan [12].

6. Conclusions

This study has demonstrated new approach for oil spill detection in multiSAR data using genetic algorithms. The RADARSAT-2 SAR and ENVISAT ASAR along the Gulf of Mexico and Singapore Straits are involved in this study. The study shows that crossover process, and the fitness function generated accurate pattern of oil slick in multiSAR data. Further, the study also shows that genetic algorithm provides accurate pattern of oil slick in SAR data. This shown by 90% for oil spill, 3% look–alike and 7% for sea roughness using the receiver –operational characteristics (ROC) curve. The Genetic algorithm also shows excellent performance in both RADARSTA-2 and ENVISAT ASAR data. In conclusion, Genetic Algorithm can be used as automatic detection tool for oil spill in multiSAR satellite data such as RADARSAT-2 SAR and ENVISAT ASAR.

Author details

Maged Marghany*

Institute of Geospatial and Science Technology (INSTEG), University of Technology, Malaysia

References

[1] Adam, J.A.: Specialties: Solar Wings, Oil Spill Avoidance, *On-Line Patterns.* IEEE Spect. 32: (1995) 87--95

[2] Aggoune M.E., Atlas L.E., Cohn D.A., El-Sharkawi, M.A. and Marks, R. J.: Artificial Neural Networks For Power System Static Security Assessment. IEEE Int. Sym. on Cir. and Syst.. Portland, Oregon. (1989) 490--494

[3] Brekke, C. and Solberg, A.: Oil Spill Detection by Satellite Remote Sensing. Rem. Sens. of Env. 95(2005)1--13

[4] Fiscella B., Giancaspro A., Nirchio, F., Pavese, P. and Trivero, P.: Oil Spill Detection Using Marine SAR Images. Int. J. of Rem. Sens. 21: (2000) 3561--3566

[5] Frate, F. D., Petrocchi, A., Lichtenegger, J. and Calabresi, G.: Neural Networks for Oil Spill Detection Using ERS-SAR Data. IEEE Tran. on Geos. and Rem. Sens. 38: (2000) 2282--2287

[6] Hect-Nielsen, R.: Theory of the Back Propagation Neural Network. Proc. of the Int. Joint Conf. on Neu. Net. IEEE Press, I: (1989) 593--611

[7] Marghany,M. and Hashim,M.: Comparative algorithms for oil spill detection from multi mode RADARSAT-1 SAR satellite data. Lecture Notes in Computer Science. D. Taniar et al. (Eds.). Computational Science and Its Applications – ICCSA 2011, 6783: (2011) 318--329

[8] Marghany, M.: RADARSAT Automatic Algorithms for Detecting Coastal Oil Spill Pollution. Int. J. of App. Ear. Obs. and Geo. 3: (2001) 191--196

[9] Marghany, M.: RADARSAT for Oil spill Trajectory Model. Env. Mod. and Sof. 19: (2004) 473--483

[10] Marghany, M., Cracknell, A. P. and Hashim, M.: Modification of Fractal Algorithm for Oil Spill Detection from RADARSAT-1 SAR Data. Int. J. of App. Ear. Obs. and Geo. 11: (2009) 96--102

[11] Marghany, M., Cracknell, A. P. and Hashim, M.: Comparison between Radarsat-1 SAR Different Data Modes for Oil Spill Detection by a Fractal Box Counting Algorithm. Int. J. of Dig. Ear. 2: (2009) 237--256

[12] Marghany, M., Hashim, M. and Cracknell, A.P.: Fractal Dimension Algorithm for Detecting Oil Spills Using RADARSAT-1 SAR. In Gervasi O. and Gavrilova M. (Eds.): LNCS, Springer-Verlag Berlin Heidelberg Part I: (2007) 1054--1062

[13] Marghany, M. and Hashim, M.: Texture Entropy Algorithm for Automatic Detection of Oil Spill from RADARSAT-1 SAR data. Int. J. of the Phy. Sci. 5: (2010) 1475--1480

[14] Michael, N. :Artificial Intelligence: A guide to Intelligent Systems. 2nd editon, Harlow, England: Addison Wesley (2005)

[15] Migliaccio, M., Gambardella, A. and Tranfaglia, M.: SAR Polarimetry to Observe Oil Spills. IEEE Tran. on Geos. and Rem. Sen. 45: (2007) 506--511

[16] Mohamed, I. S, Salleh, A.M. and Tze, L.C.: Detection of Oil Spills in Malaysian Waters from RADARSAT Synthetic Aperture Radar Data and Prediction of Oil Spill Movement. Proc. of 19th Asi. Conf. on Rem. Sen. Hong Kong, China, 23–27 November. Asian Remote Sensing Society, Japan, 2: (1999) 980--987

[17] Provost, F. and Fawcett, T.: Robust classification for imprecise environments. Mach. Lear.42: (2001)203--231

[18] Samad, R., and Mansor, S.B.: Detection of Oil Spill Pollution Using RADARSAT SAR Imagery. CD Proc. of 23rd Asi. Conf. on Rem. Sens. Birendra International Convention Centre in Kathmandu, Nepal, November 25-29, 2002, Asian Remote Sensing (2002)

[19] Skrunes, S., C. Brekke, and T. Eltoft, "An Experimental Study on Oil Spill Characterization by Multi-Polarization SAR," in Proc. European Conference on Synthetic Aperture Radar, Nuremberg, Germany (2012) 139--142

[20] Topouzelis, K., Karathanassi, V., Pavlakis, P. and Rokos, D.: Potentiality of Feed-Forward Neural Networks for Classifying Dark Formations to Oil Spills and Look-alikes. Geo. Int. 24, (2009)179--19

[21] Topouzelis, K., Karathanassi, V., Pavlakis, P. and Rokos, D.: Detection and Discrimination between Oil Spills and Look-alike Phenomena through Neural Networks. ISPRS J. Photo. Rem. Sens. 62: (2007) 264--270

[22] Topouzelis, K.N.: Oil Spill Detection by SAR Images: Dark Formation detection, Feature Extraction and Classification Algorithms. Sens. 8: (2008) 6642--6659

[23] Trivero, P., Fiscella, B. and Pavese, P.: Sea Surface Slicks Measured by SAR, Nuo. Cim. 24C, (2001) 99--111

[24] Trivero, P., Fiscella, B., Gomez, F., and Pavese, P.: SAR Detection and Characterization of Sea Surface Slicks. Int. J. Rem. Sen. 19: (1998) 543--548

[25] Velotto, D., M. Migliaccio, F. Nunziata, and S. Lehner, "Dual-Polarized TerraSAR-X Data for Oil-Spill Observation," IEEE Trans. Geosci. Remote Sens., 49: (2011) 4751--4762

[26] Chaiyaratana, N.; Zalzala, A.M.S: Recent developments in evolutionary and genetic algorithms: theory and applications. Genetic Algorithms in Engineering Systems: Innovations and Applications,GALESIA 97. Second International Conference On 2-4 Sept. 1997, Glasgow, (1997) 270--277

[27] Kahlouche,S., K.Achour, and M. Benkhelif: Proceedings of the 2002 WSEAS International Conferences, Cadiz, Spain, June 12-16, 2002. www.wseas.us/e-library/conferences/spain2002/papers/443-164.pdf: (2002)1--5

[28] Gautam, G., and B.B. Chaudhuri: A distributed hierarchical genetic algorithm for efficient optimization and pattern matching: Pattern Recognition Journal, 40: (2007) 212--228

[29] Sivanandam, S.N, and Deepa S.N: Introduction to Genetic Algorithms, by Springer Berlin Heidelberg New York (2008)

[30] Marghany M. Genetic Algorithm for Oil Spill Automatic Detection from Envisat Satellite Data. In Beniamino Murgante, Sanjay Misra, Maurizio Carlini, Carmelo M. Torre, Hong-Quang Nguyen, David Taniar, Bernady O. Apduhan, and Osvaldo Gervasi. Computational Science and Its Applications – ICCSA 2013, 7972, pp 587-598.

[31] Marghany M. Genetic Algorithm for Oil Spill Automatic Detection from Multisar Satellite Data. Proceedings of the 34th Asian Conference on Remote Sensing 2013. Bali – Indonesia, October 20-24, 2013. pp. SC03-671-SC0-3677.

IntechOpen